SCIENCE CHINA
Physics, Mechanics & Astronomy

•Article•

April 2019 Vol. 62 No. 4: 048211
https://doi.org/10.1007/s11433-018-9319-3

Pressure-induced Lifshitz transition in the type II Dirac semimetal $PtTe_2$

FengLiang Liu[1,2†], JiaHeng Li[3†], KeNan Zhang[3], Shang Peng[2], HuaQing Huang[3], MingZhe Yan[3], NaNa Li[2], Qian Zhang[2], SongHao Guo[2], XuJie Lü[2], Peng Cai[1,4,5], LiFeng Yin[1,4,5], ShuYun Zhou[3], WenHui Duan[3*], Jian Shen[1,4,5*], and WenGe Yang[2,6*]

[1] *State Key Laboratory of Surface Physics and Department of Physics, Fudan University, Shanghai 200433, China;*
[2] *Center for High Pressure Science and Technology Advanced Research (HPSTAR), Shanghai 201203, China;*
[3] *State Key Laboratory of Low Dimensional Quantum Physics and Department of Physics, Tsinghua University, Beijing 100084, China;*
[4] *Institute for Nanoelectronic Devices and Quantum Computing, Fudan University, Shanghai 200433, China;*
[5] *Collaborative Innovation Center of Advanced Microstructures, Nanjing 210093, China;*
[6] *High Pressure Synergetic Consortium (HPSynC), Geophysical Laboratory, Carnegie Institution of Washington, Argonne IL 60439, USA*

Received September 16, 2018; accepted October 30, 2018; published online December 29 2018

Numerous exotic properties have been discovered in Dirac Semimetals (DSMs) and Weyl Semimetals (WSMs). In a given DSM/WSM, the Dirac/Weyl nodes usually coexist with other bulk states, making their respective contribution elusive. In this work, we distinguish the role of bulk states from the tilted Dirac nodes on the transport properties in DSMs. Specifically, we applied pressure to a type-II DSM material, $PtTe_2$, and studied its pressure modified electronic and lattice structure systematically by using *in situ* transport measurements and X-ray diffraction (XRD). A pressure-induced transition at about 20 GPa is revealed in the transport properties, while the layered lattice structure is robust against pressure as illustrated in XRD measurement results. Density functional theory (DFT) calculations suggest that this is originated from the Lifshitz transition in the bulk states. Our findings provide evidence to identify the bulk states' influence on transport from the topologically-protected DSM states in the DSM material.

Dirac semimetals, diamond anvil cells, X-ray diffraction, transport measurement, band structure calculation

PACS number(s): 07.35.+k, 61.10.Nz, 61.50.Ks, 81.30.Hd, 71.20.-b, 73.20.At

Citation: F. L. Liu, J. H. Li, K. N. Zhang, S. Peng, H. Q. Huang, M. Z. Yan, N. N. Li, Q. Zhang, S. H. Guo, X. J. Lü, P. Cai, L. F. Yin, S. Y. Zhou, W. H. Duan, J. Shen, and W. G. Yang, Pressure-induced Lifshitz transition in the type II Dirac semimetal $PtTe_2$, Sci. China-Phys. Mech. Astron. **62**, 048211 (2019), https://doi.org/10.1007/s11433-018-9319-3

1 Introduction

Dirac semimetals (DSMs) and Weyl semimetals (WSMs) have attracted intensive interests in the condensed matter physics community in the last several years [1-7]. The Dirac or Weyl fermions are basic concepts in high-energy physics which can be realized in these three-dimensional topological semimetals with unique physical properties, such as large unsaturated linear magneto-resistance (MR) [3], negative MR [4], chiral anomaly [5], etc. Based on the linear kinetic term T(K) and potential component U(K) in the generic Hamiltonian, DSMs and WSMs can be categorized into two

†These authors contributed equally to this work.
*Corresponding authors (WenGe Yang, email: yangwg@hpstar.ac.cn; WenHui Duan, email: dwh@phy.tsinghua.edu.cn; Jian Shen, email: shenj5494@fudan.edu.cn)

types [6,7]. In type-I DSMs, isolated Dirac points were expected to be near the Fermi surface, and many novel phenomena were observed, e.g., large MR [8-11], negative MR [11] and even tuned superconducting transition [12]. When the T(K) is larger than the U(K) along a certain moment direction, a strongly tilted Dirac cone emerges, in which the Dirac points are located far away from the Fermi level and form a type-II WSM [13] or DSM, such as the $PtTe_2$ [14], $PtSe_2$ [15,16] and $PdTe_2$ family [17-22]. There is a lack of observation on such anisotropy in transport properties, due to the defect or boundary scattering in the presence of both bulk and topologically-protected charge carriers. So far few investigations have been done to determine the role that bulk states near the Fermi energy from topologically-protected states have played in the transport behaviors of the DSMs.

The newly discovered group-X chalcogenide-based compounds MX_2 (M=Pd, Pt, X=Te, Se), a typical type-II DSM group with tilted Dirac nodes located far away from the Fermi surface, gives us a new opportunity to study the importance of the bulk states in their transport properties. The 3D Dirac node located near 0.8 eV below the Fermi surface in $PtTe_2$ [14] makes $PtTe_2$ the best choice for investigating the contributions of the bulk states to the transport behavior in the DSMs. Pressure has been widely used as an important controlling parameter to fine tune both lattice and electronic structures [23-32]. So far, a great amount of exotic physical phenomena has been reported in the DSMs and WSMs under high pressures, including pressure-induced phase transition [25], superconducting transition [26-30], metal-insulator transition [31] and novel WSM [32] phases.

In this study, we employ the synchrotron X-ray diffraction and magneto-transport measurements, coupled with high pressure Diamond Anvil Cell (DAC) techniques, to investigate the systematic evolution of the crystal structure and physical properties of $PtTe_2$ under quasi-hydrostatic pressures up to 53.6 GPa. Transport measurements indicate that, upon increasing pressure to around 20 GPa, a resistivity anomaly appears in conjunction with the dramatic decrease of magnetoresistance and electron carrier density. These changes strongly suggest a transition in $PtTe_2$'s electronic origin, given the crystalline structure being stable even up to 50.2 GPa. Combining density functional theory (DFT) calculations and transport measurements, we conclude that the observed transition occurs after the Lifshitz transition instead of the DSM state annihilation. Our results indicate that the anisotropically-compressed DSM material $PtTe_2$ is significantly influenced by the bulk states near Fermi surface rather than the topologically-protected electronic states.

2 Experimental methods

High quality single crystal $PtTe_2$ was synthesized by using self-flux method reported previously [14]. For high pressure magneto-transport measurements, Pt wires were in contact with the crystalline sample using standard four-probe van der Pauw geometry, and the diamond anvil cell was made of non-magnetic Be-Cu alloy. The synchrotron X-ray diffraction on the same batch sample was performed using Mao-Bell type diamond anvil cell [33]. In all these experiments, the pressure is implemented at room temperature and calibrated by the ruby fluorescence method [34]. *In situ* high pressure angle dispersive X-ray diffraction (XRD) was performed in the synchrotron radiation beamline, with the incident X-ray wavelength 0.3066 Å for room temperature experiment up to 50.2 GPa at sector 16-BM-D of Advanced Photon Source (APS), Argonne National Lab (ANL), and the incident X-ray wavelength 0.4066 Å at sector 16-ID-B of APS, ANL for the low temperature XRD measurement. The diffraction patterns were converted into one dimensional raw data by the Dioptas software [35] and further analysis in the GSAS [36] software by using the Rietveld refinement [37] method, aiming to get the structure information.

Theoretical calculation on the electronic band structure was performed by using the Vienna *ab initio* Simulation Package (VASP) [38]. The Perdew-Burke-Ernzerhof-type generalized gradient approximation (GGA) and the projector augmented wave (PAW) method were employed, and spin-orbit coupling was included self-consistently in the calculation. The lattice parameters are taken from the high pressure X-ray diffraction measurement done at room temperature, but the atoms inside are fully relaxed until the force on each atom is less than 0.001 eV/Å. A plane-wave wave basis set with kinetic energy cutoff of 400 eV is used for both Platinum and Tellurium element. 12×12×9 Monkhorst-Pack *K*-point mesh is used in the structure relaxation calculations, and 18×18×15 Monkhorst-Pack *k*-point mesh is used for self-consistent calculations.

3 Experimental results

Figure 1(a) shows the temperature dependence of resistance (*R*-*T*) of a $PtTe_2$ single crystal at temperature between 2 and 300 K at various pressures in a Physical Property Measurement System (PPMS, Quantum Design Inc.). In the entire pressure range, the $PtTe_2$ behaves as a metal. Its residual resistance was defined at 2 K, which increases with increasing pressure (Figure 1(b)). The increasing slope of the residual resistance with increasing pressure jumps to a larger value at around 20 GPa, as shown in Figure 1(b). When the pressure is below 20 GPa, the *R*-*T* curves are nearly linear in the temperature range between 30 and 300 K, which is similar to the case at ambient pressure [39]. At pressures above 20 GPa, the *R*-*T* curves are clearly nonlinear which is best demonstrated by subtracting the residual resistance of the *R*-

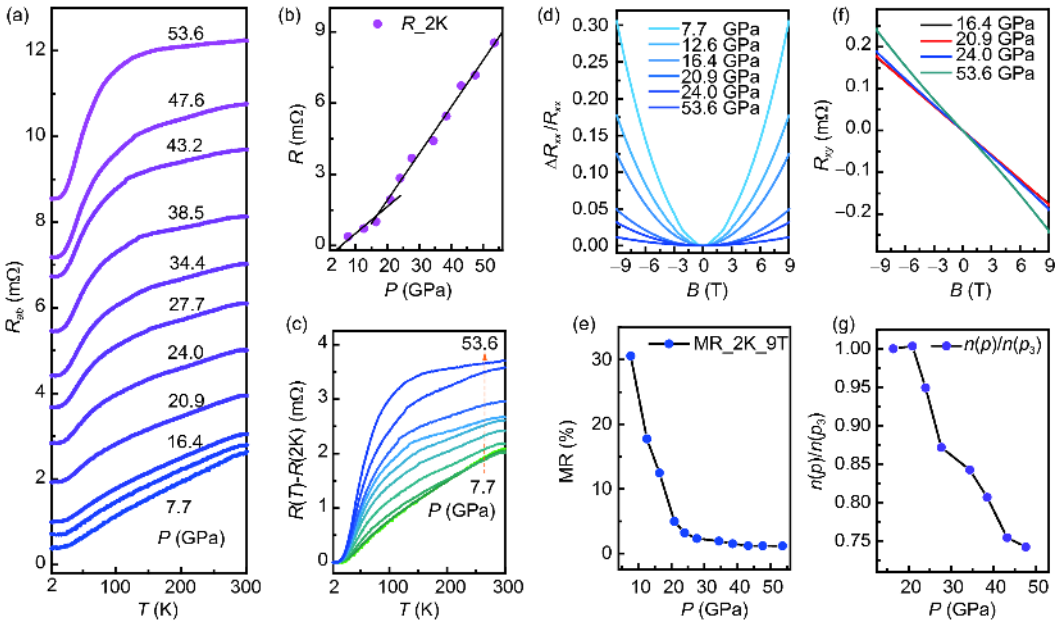

Figure 1 (Color online) High pressure transport studies of $PtTe_2$. (a) Temperature dependence of in-plane (*a*-*b* plane) resistances at a series of pressure points without magnetic field; (b) pressure dependence of residual resistance at 2 K (the two black lines with different slopes represent the transition in pressure dependent residual resistance around 20 GPa); (c) temperature dependence of in-plane (*a*-*b* plane) resistance after subtracting the residual resistance, defined as $R(T)$-$R(2K)$; (d) the magnetic field dependence of high pressure resistance up to 9 T at 2 K, with a magnetic field applied along the *c*-axis direction (define $\Delta R_{xx}=R_{xx}(B)-R_{xx}(0\ T)$, $R_{xx}=R_{xx}$ (0 T)); (e) magneto-resistance (MR = $\Delta R_{xx}/R_{xx}$) as a function of pressure at 2 K and 9 T; (f) the magnetic field dependence of high pressure hall resistance at 2 K, R_{xy} defined as hall resistance; (g) relative electronic carrier density ($n(p)/n(p_3)$, p_3=16.4 GPa) evolutions of pressure.

T curves at each pressure (Figure 1(c)). The deviation of linearity for the *R*-*T* curves at pressures above 20 GPa underlies a pressure driven transition in $PtTe_2$ around 20 GPa, which is also captured in Figure 1(b).

Figure 1(d) shows the magnetic field dependence of magnetoresistance (MR) at 2 K for different pressures. At each pressure level, the MR keeps positive, increasing nonlinearly with field showing no sign of saturation up to 9 T. This suggests that $PtTe_2$ is not a system with electron-hole compensation [39], which should exhibit a linear dependence of MR on magnetic field [40]. Figure 1(e) shows the MR values measured at 9 T as a function of pressure. The MR (9 T) values fall rapidly from near 30% at 7.7 GPa to 5% at 20.9 GPa, above which MR decreases much slower. The noticeable change in the decreasing rate of MR with increasing pressure at the critical pressure (P_c) ~20 GPa again marks a transition in $PtTe_2$.

Such transition was further evidenced by pressure dependence of carrier density. To obtain the carrier density, field-dependent Hall resistance is measured at various pressures as shown in Figure 1(f). Clearly, the $PtTe_2$ system is dominated by electron-like carriers. The carrier densities measured at different pressures are normalized by that measured at 16.3 GPa, as shown in Figure 1(g). The relative carrier density changes little below P_c~20 GPa but drops sharply from 20.9 to 47.6 GPa. The sudden change of the carrier density provides yet another evidence for the transition in $PtTe_2$ at the critical pressure P_c~ 20 GPa.

To elucidate the origin of this pressure driven transition, we examine the structural stability of the $PtTe_2$ by using high-pressure synchrotron X-ray diffraction (XRD) measurement at both room and low temperatures. The pressure dependence of XRD profiles at 300 K is shown in Figure 2(a). The measurements were conducted at the pressures ranging from 4.4 to 50.2 GPa. The XRD profiles can be well indexed by the original CdI_2-type (1*T*) structure with the space group ($P\bar{3}m1$), the same as the ambient structure reported previously [14]. As pressure increases, the XRD profiles evolve smoothly without any abrupt changes. It demonstrates that the ambient phase keeps stable up to 50.2 GPa at room temperature. At low temperature, this phase is also stable up to 30.1 GPa as illustrated in the smooth evolution of XRD patterns at 85 K under various pressures (Figure 2(b)). The detailed Rietveld refinement analyses of the XRD patterns are shown in Figures S2-S5 in the Supporting Information, suggesting that the lattice symmetry and space group are also stable. The hexagonal lattice structure of $PtTe_2$ is schematically shown in Figure 2(c), which is very robust against pressure.

To quantify the pressure effect on lattice parameters, we applied Rietveld refinement analyses on the XRD profiles at room temperature to determine the lattice constants at various pressures and plotted the results in Figure 2(d). The in-plane lattice (*a*) contraction is much smaller than the out-plane lattice (*c*) contraction. Up to 50.2 GPa, the in-plane lattice is contracted by 4.4% while the out-plane lattice is

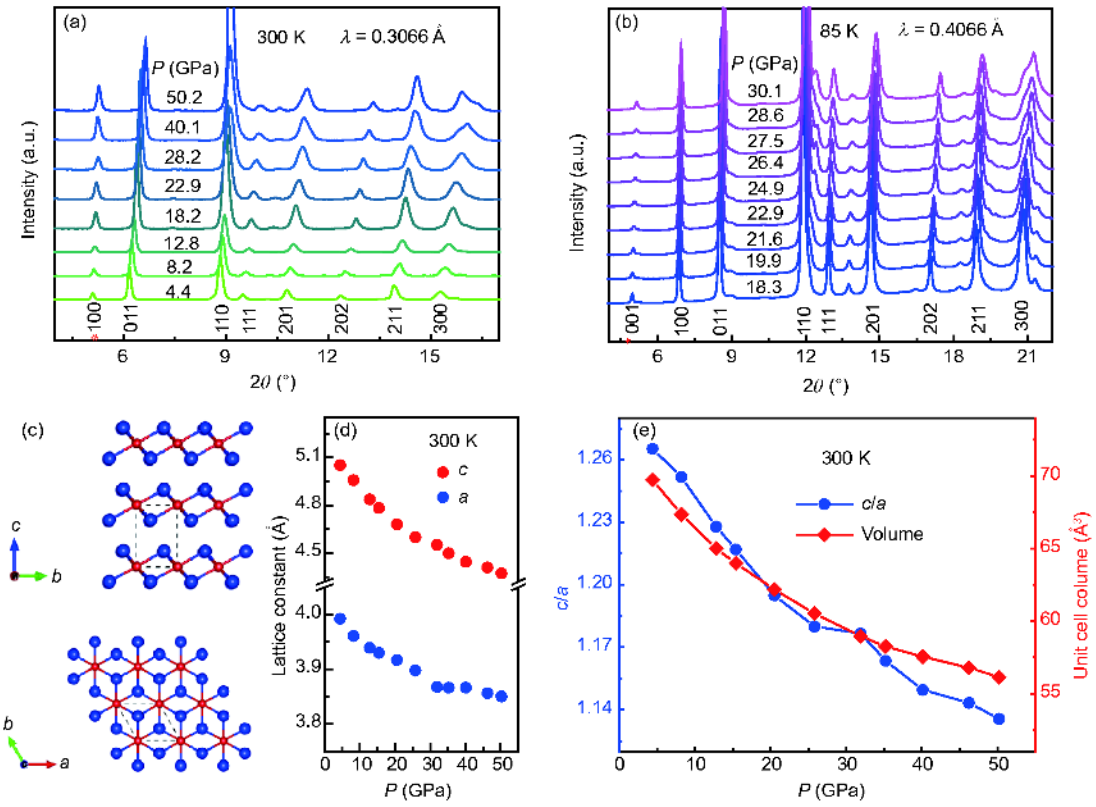

Figure 2 (Color online) Structure evolution of $PtTe_2$ probed by synchrotron XRD under high pressure. (a) Powder XRD patterns collected at room temperature, up to 50.2 GPa (incident X-ray wavelength=0.3066 Å); (b) powder XRD patterns collected at 85 K, within 30.1 GPa (incident X-ray wavelength = 0.4066 Å); (c) sideview (up) and topview (down) of lattice structure in $PtTe_2$ (Pt atom labels with red color, and Te atom labels with blue color); (d) the lattice parameters (*a*, *c*) derived from Rietveld refinement; (e) high pressure evolution of *c*/*a* ratio and unit cell volume at room temperature.

contracted by 16.3% (Figure S6). The anisotropic contraction is clearly revealed by the pressure-dependent *c*/*a* ratio (Figure 2(e)). This strong anisotropic compressibility can be explained by the fact that the covalent bonding in intralayer is much stronger than the interlayer van der Waals bonding in $PtTe_2$. The pressure-dependent unit-cell volume further reveals the continuous evolution of lattice parameter of $PtTe_2$ (Figure 2(e)). These results confirm that the $PtTe_2$ is robust under pressure.

The pressure dependence of the electronic structure is studied by the DFT calculations. As the pressure increases, there are two significant changes in the electronic band structure of $PtTe_2$. First, the tilted Dirac node moves towards *A*-point in the BZ as the pressure rises gradually up to 10 GPa (Figure 3(a) and (b)). Once the pressure is over 10 GPa, a gap opens at the Dirac node, (Figure 3(c)). The annihilation of Dirac node is a natural consequence of the degeneracy at *A*-point, which means that two separated nodes meet at this point. There are not any topological nodes when the pressure is above 10.2 GPa, showing a topological phase transition driven by pressure. Besides, at the same pressure range of Dirac node annihilation, the conduction bands at *L*-point are lifted when the pressure is over 6.3 GPa, leading to a Lifshitz transition for the Fermi surface topology at *L*-point (Figure 3(a) and (b)). Second, the conduction bands at *K*-point are lifted when the pressure is over 18.2 GPa, leading to a Lifshitz transition for the Fermi surface topology at *K*-point (Figure 3(d) and (e)). These conduction bands at *K*-point are trivial bulk states without topological protection. Above 18.2 GPa, the Fermi surface crosses these trivial bands at low pressure and does not intersect with these bands (Figure 3(f)). To further visualize this Lifshitz transition, the Fermi surface topology at the plane k_c=0 are displayed (Figure 4). Around *K*-point, the single Fermi surface at low pressure is transformed into three separated pockets. Above 20.5 GPa, there are not further significant changes in the calculated band structure and associated Fermi surfaces. Please refer to Figures S7-S9 for more details.

4 Discussions

The transition in transport properties at $P_c \sim 20$ GPa does not originate from the structural transition because the crystal structure of $PtTe_2$ is very robust through the entire pressure range. This is also consistent with the fact that the evolution of transport properties is rather smooth, while structural

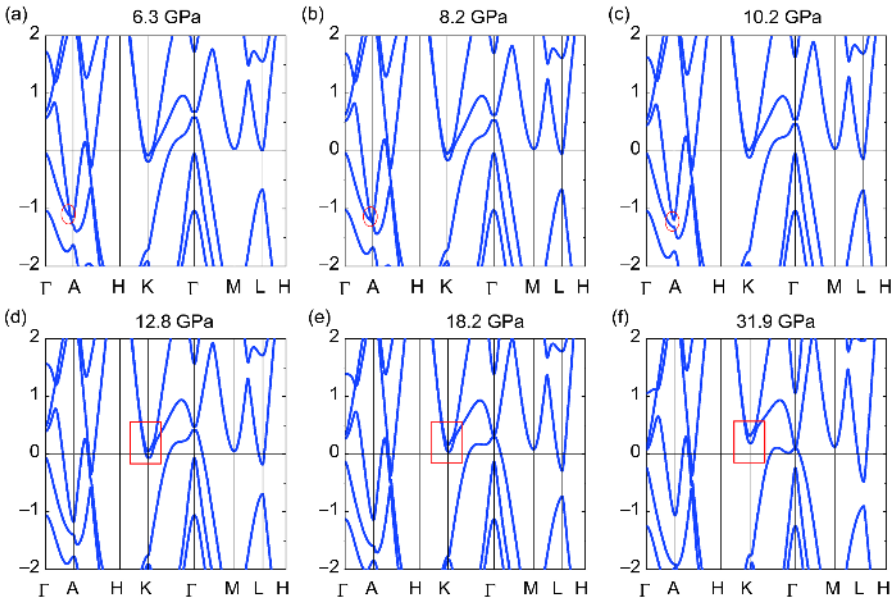

Figure 3 (Color online) DFT calculation of electronic band structure along the Γ-A-H-K-Γ-M-L-H path at several different pressure points (6.3, 8.2, 10.2, 12.8, 18.2 and 31.9 GPa). Pressure dependent evolution of Dirac semimetal state (marked by red circle in (a)-(c)) and trivial electronic band pocket located at *K*-point (marked by red square in (d)-(f)).

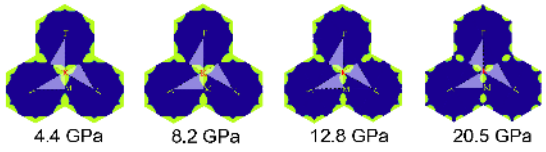

Figure 4 (Color online) Fermi surface evolution of pressurized $PtTe_2$ at 4.4, 8.2, 12.8 and 20.5 GPa. The yellow areas demonstrate the pocket topology of Fermi surface.

phase transition usually results in a dramatic change in electronic properties accompanied with hysteresis [41]. In this sense, the transition is of an electronic origin. It can be attributed to the Lifshitz transition of the bulk states. The annihilation of Dirac nodes at 10 GPa shows no dramatic effects on transport properties because the topologically-protected Dirac node [14] is far away from the Fermi energy. In addition, during the Lifshitz transition at *L*-point, the R-T behavior is still linearly dependent on temperature between 30 and 300 K, showing no obvious changes when compared with the ambient one [39]. There is no evidence of transitions in transport during the pressure range of Dirac nodes annihilation and Lifshitz transition at *L*-point. However, a dramatic transition occurs around 20 GPa as revealed by *R*-*T*, MR and Hall measurements in transport, just after the pressure range of Liftshitz transition at *K*-point, which gives a consistent scenario in the view of DFT calculation and experiment measurement. Definitely, the dramatic decrease of charge carrier density above P_c = 20 GPa strongly supports the Liftshiz transition scenario. More importantly, the notable magnetoresistance changes occurred during the Liftshitz transition of bulk states suggest that the contribution of bulk states to magneto-transport properties should also be considered in other systems with topologic orders.

We now turn to discuss the origin of the resistivity anomaly above 20 GPa for $PtTe_2$. The effect of pressure-induced defects can be first ruled out because the residual resistance of $PtTe_2$ decreases with decreasing pressure, which does not occur for defects (Figure S1(a)). In some of its cousin systems, such as $IrTe_2$ and $PdTe_2$, upon cooling or increasing pressure there are structural phase transitions or Te dimerizations driven by the electronic instability [42]. It was suggested that the electronic order could be a cause of the resistivity anomaly. However, because electron ordering together with the electron-lattice coupling usually leads to structural phase transitions which are absent in $PtTe_2$, we believe that the resistivity anomaly in $PtTe_2$ above 20 GPa is not the result of electronic order. In contrast to the sharp transition for electron ordering, there is not a clear transition temperature for the resistivity anomaly in $PtTe_2$. The electronic structure of $PtTe_2$ is tuned to the boundary of Liftshitz transition by pressure. Near the transition boundary, the electronic structure is very sensitive to the temperature. Therefore, the resistivity anomaly around P_c = 20 GPa can be ascribed to the temperature-induced Lifshitz transition. Intriguingly, such temperature induced Lifshitz transition is also evidenced by similar resistivity anomaly with broad transition temperature in another topological material $ZrTe_5$ [43,44]. However, at the pressures far above P_c, the Fermi surface of $PtTe_2$ would be far away from critical point for the geometric topology transition, and thus, the temperature-in-

duced Lifshitz transition would be no longer responsible to the resistivity anomaly.

In addition to the resistivity anomaly at high pressure far above P_c, the dramatic increase of resistivity upon pressure is also puzzling. In usual cases, residual resistivity can be simply related to the mean free path and Fermi surface in the simple version of Boltzmann equation [45]. From 16.4 GPa up to 50.2 GPa, the charge carrier only decreases to 75% while the residual resistance increases almost one order of magnitude, indicating that the mean free path deceases significantly with increasing pressure. Recently, an unexpected Fermi pocket is observed in $PtTe_2$ at ambient pressure by the de Haas-van Alphen effects, implying strong electron correlations in this specific system [46]. The effect of additional Fermi pocket and electronic correlations under pressure could be very complex and may be responsible to the pressure induced resistivity anomaly. This brings up another topic for future investigation.

5 Conclusions

In conclusion, we propose that the Lifshitz transition in the trivial bulk states, rather than the topologically-protected Dirac nodes, plays a significant role in transport properties of the pressurized type-II Dirac semimetal $PtTe_2$. XRD measurements reveal that the lattice is anisotropically compressed, while its structure symmetry is stable up to 50.2 GPa. Transport measurement and DFT calculation suggest that the transition in the transport properties is originated from the Lifshitz transition in the bulk states. The quantitative understanding of the Lifshitz transition on such systems with complex Fermi surfaces will inspire further investigations on the detailed parameters (such as scattering rate) for each pockets. To the best of our knowledge, this is the first work to demonstrate the significance of bulk states to its transport properties in the Dirac semimetals. In addition, the findings of pressure driven Lifshitz transition and resistance anomaly in DSM motivates further studies and discussions of electron correlations and electron-lattice coupling effect in the topological materials.

Supporting Information

The supporting information is available online at phys.scichina.com and http://link.springer.com/journal/11433. The supporting materials are published as submitted, without typesetting or editing. The responsibility for scientific accuracy and content remains entirely with the authors.

This work was supported by the National Key Research Program of China (Grant No. 2016YFA0300702), the National Basic Research Program of China (Grant No. 2014CB921104), the Shanghai Municipal Natural Science Foundation (Grant Nos. 18JC1411400, 18ZR1403200, and 17ZR1442400), the National Natural Science Foundation of China (Grant No. U1530402), China Postdoctoral Science Foundation (Grant No. 2017M610221), Shanghai Sailing Program (Grant No. 17YF1429000), the National Postdoctoral Program for Innovative Talents (Grant No. BX201600036), and the National Natural Science Foundation of China (Grant No. 11674188). We acknowledge Dr. LiLi Zhang, Dr. ShangMing He, and Dr. AiGuo Li of 15U1 at SSRF, Dr. DongZhou Zhang of 13-BMC at GSECARS, APS, and Dr. Jesse Smith, Curtis Kenney-Benson at HPCAT, APS for the technical supports on the high pressure XRD experiment. Gas loading by Sergey N. Tkachev is also acknowledged. 13BM-C operation is supported by COMPRES through the Partnership for Extreme Crystallography (PX2) project, under NSF Cooperative Agreement EAR 11-57758. HPCAT operations are supported by DOE-NNSA under Award No. DE-NA0001974 and DOE-BES under Award No. DE-FG02-99ER45775, with partial instrumentation funding by NSF. APS is supported by DOE-BES, under Contract No. DE-AC02-06CH11357.

1 X. Wan, A. M. Turner, A. Vishwanath, and S. Y. Savrasov, Phys. Rev. B **83**, 205101 (2011), arXiv: 1007.0016.
2 H. Weng, C. Fang, Z. Fang, B. A. Bernevig, and X. Dai, Phys. Rev. X **5**, 011029 (2015), arXiv: 1501.00060.
3 C. Shekhar, A. K. Nayak, Y. Sun, M. Schmidt, M. Nicklas, I. Leermakers, U. Zeitler, Y. Skourski, J. Wosnitza, Z. Liu, Y. Chen, W. Schnelle, H. Borrmann, Y. Grin, C. Felser, and B. Yan, Nat. Phys. **11**, 645 (2015), arXiv: 1502.04361.
4 F. Arnold, C. Shekhar, S. C. Wu, Y. Sun, R. D. Dos Reis, N. Kumar, M. Naumann, M. O. Ajeesh, M. Schmidt, A. G. Grushin, J. H. Bardarson, M. Baenitz, D. Sokolov, H. Borrmann, M. Nicklas, C. Felser, E. Hassinger, and B. Yan, Nat. Commun. **7**, 11615 (2016), arXiv: 1506.06577.
5 Q. Li, D. E. Kharzeev, C. Zhang, Y. Huang, I. Pletikosić, A. V. Fedorov, R. D. Zhong, J. A. Schneeloch, G. D. Gu, and T. Valla, Nat. Phys. **12**, 550 (2016), arXiv: 1412.6543.
6 H. Weng, X. Dai, and Z. Fang, J. Phys.-Condens. Matter **28**, 303001 (2016), arXiv: 1603.04744.
7 B. Yan, and C. Felser, Annu. Rev. Condens. Matter Phys. **8**, 337 (2017), arXiv: 1611.04182.
8 T. Liang, Q. Gibson, M. N. Ali, M. Liu, R. J. Cava, and N. P. Ong, Nat. Mater. **14**, 280 (2015), arXiv: 1404.7794.
9 M. Neupane, S. Y. Xu, R. Sankar, N. Alidoust, G. Bian, C. Liu, I. Belopolski, T. R. Chang, H. T. Jeng, H. Lin, A. Bansil, F. Chou, and M. Z. Hasan, Nat. Commun. **5**, 3786 (2014), arXiv: 1309.7892.
10 L. P. He, X. C. Hong, J. K. Dong, J. Pan, Z. Zhang, J. Zhang, and S. Y. Li, Phys. Rev. Lett. **113**, 246402 (2014), arXiv: 1404.2557.
11 J. Xiong, S. K. Kushwaha, T. Liang, J. W. Krizan, M. Hirschberger, W. Wang, R. J. Cava, and N. P. Ong, Science **350**, 413 (2015).
12 L. He, Y. Jia, S. Zhang, X. Hong, C. Jin, and S. Li, npj Quant. Mater. **1**, 16014 (2016).
13 A. A. Soluyanov, D. Gresch, Z. Wang, Q. S. Wu, M. Troyer, X. Dai, and B. A. Bernevig, Nature **527**, 495 (2015), arXiv: 1507.01603.
14 M. Yan, H. Huang, K. Zhang, E. Wang, W. Yao, K. Deng, G. Wan, H. Zhang, M. Arita, H. Yang, Z. Sun, H. Yao, Y. Wu, S. Fan, W. Duan, and S. Zhou, Nat. Commun. **8**, 257 (2017), arXiv: 1607.03643.
15 H. Huang, S. Zhou, and W. Duan, Phys. Rev. B **94**, 121117(R) (2016), arXiv: 1607.07965.
16 K. Zhang, M. Yan, H. Zhang, H. Huang, M. Arita, Z. Sun, W. Duan, Y. Wu, and S. Zhou, Phys. Rev. B **96**, 125102 (2017), arXiv: 1703.04242.
17 H. J. Noh, J. Jeong, E. J. Cho, K. Kim, B. I. Min, and B. G. Park, Phys. Rev. Lett. **119**, 016401 (2017), arXiv: 1612.06946.
18 R. C. Xiao, P. L. Gong, Q. S. Wu, W. J. Lu, M. J. Wei, J. Y. Li, H. Y. Lv, X. Luo, P. Tong, X. B. Zhu, and Y. P. Sun, Phys. Rev. B **96**, 075101 (2017), arXiv: 1705.05708.
19 H. Leng, C. Paulsen, Y. K. Huang, and A. de Visser, Phys. Rev. B **96**, 220506(R) (2017), arXiv: 1710.03862.
20 C. Cheng, J. T. Sun, M. Liu, X. R. Chen, and S. Meng, Phys. Rev. Mater. **1**, 074804 (2017).

21 Y. Li, Y. Xia, S. A. Ekahana, N. Kumar, J. Jiang, L. Yang, C. Chen, C. Liu, B. Yan, C. Felser, G. Li, Z. Liu, and Y. Chen, Phys. Rev. Mater. **1**, 074202 (2017).

22 M. A. ElGhazali, P. G. Naumov, H. Mirhosseini, V. Süß, L. Müchler, W. Schnelle, C. Felser, and S. A. Medvedev, Phys. Rev. B **96**, 060509 (R) (2017).

23 H. K. Mao, B. Chen, J. Chen, K. Li, J. F. Lin, W. Yang, and H. Zheng, Matter Radiat. Extrem. **1**, 59 (2016).

24 G. H. Han, D. L. Duong, D. H. Keum, S. J. Yun, and Y. H. Lee, Chem. Rev. **118**, 6297 (2018).

25 Y. Zhou, X. Chen, N. Li, R. Zhang, X. Wang, C. An, Y. Zhou, X. Pan, F. Song, B. Wang, W. Yang, Z. Yang, and Y. Zhang, AIP Adv. **6**, 075008 (2016).

26 D. Kang, Y. Zhou, W. Yi, C. Yang, J. Guo, Y. Shi, S. Zhang, Z. Wang, C. Zhang, S. Jiang, A. Li, K. Yang, Q. Wu, G. Zhang, L. Sun, and Z. Zhao, Nat. Commun. **6**, 7804 (2015), arXiv: 1502.00493.

27 X. C. Pan, X. Chen, H. Liu, Y. Feng, Z. Wei, Y. Zhou, Z. Chi, L. Pi, F. Yen, F. Song, X. Wan, Z. Yang, B. Wang, G. Wang, and Y. Zhang, Nat. Commun. **6**, 7805 (2015), arXiv: 1501.07394.

28 Y. Qi, P. G. Naumov, M. N. Ali, C. R. Rajamathi, W. Schnelle, O. Barkalov, M. Hanfland, S. C. Wu, C. Shekhar, Y. Sun, V. Süß, M. Schmidt, U. Schwarz, E. Pippel, P. Werner, R. Hillebrand, T. Förster, E. Kampert, S. Parkin, R. J. Cava, C. Felser, B. Yan, and S. A. Medvedev, Nat. Commun. **7**, 11038 (2016), arXiv: 1508.03502.

29 Y. Qi, W. Shi, P. G. Naumov, N. Kumar, W. Schnelle, O. Barkalov, C. Shekhar, H. Borrmann, C. Felser, B. Yan, and S. A. Medvedev, Phys. Rev. B **94**, 054517 (2016), arXiv: 1602.08616.

30 Y. Zhou, J. Wu, W. Ning, N. Li, Y. Du, X. Chen, R. Zhang, Z. Chi, X. Wang, X. Zhu, P. Lu, C. Ji, X. Wan, Z. Yang, J. Sun, W. Yang, M. Tian, Y. Zhang, and H. K. Mao, Proc. Natl. Acad. Sci. USA **113**, 2904 (2016), arXiv: 1505.02658.

31 S. Zhang, Q. Wu, L. Schoop, M. N. Ali, Y. Shi, N. Ni, Q. Gibson, S. Jiang, V. Sidorov, W. Yi, J. Guo, Y. Zhou, D. Wu, P. Gao, D. Gu, C. Zhang, S. Jiang, K. Yang, A. Li, Y. Li, X. Li, J. Liu, X. Dai, Z. Fang, R. J. Cava, L. Sun, and Z. Zhao, Phys. Rev. B **91**, 165133 (2015), arXiv: 1410.3213.

32 Y. Zhou, P. Lu, Y. Du, X. Zhu, G. Zhang, R. Zhang, D. Shao, X. Chen, X. Wang, M. Tian, J. Sun, X. Wan, Z. Yang, W. Yang, Y. Zhang, and D. Xing, Phys. Rev. Lett. **117**, 146402 (2016).

33 H. K. Mao, P. M. Bell, K. J. Dunn, R. M. Chrenko, and R. C. DeVries, Rev. Sci. Instrum. **50**, 1002 (1979).

34 H. K. Mao, J. Xu, and P. M. Bell, J. Geophys. Res. **91**, 4673 (1986).

35 C. Prescher, and V. B. Prakapenka, High Pressure Res. **35**, 223 (2015).

36 B. H. Toby, and R. B. Von Dreele, J Appl Cryst. **46**, 544 (2013).

37 H. M. Rietveld, J Appl Cryst. **2**, 65 (1969).

38 G. Kresse, and J. Furthmüller, Phys. Rev. B **54**, 11169 (1996).

39 D. Fu, X. Bo, F. Fei, B. Wu, M. Gao, X. Wang, M. Naveed, S. A. Shah, H. Bu, B. Wang, L. Cao, W. Zou, X. Wan, and F. Song, Phys. Rev. B **97**, 245109 (2018).

40 P. L. Cai, J. Hu, L. P. He, J. Pan, X. C. Hong, Z. Zhang, J. Zhang, J. Wei, Z. Q. Mao, and S. Y. Li, Phys. Rev. Lett. **115**, 057202 (2015), arXiv: 1412.8298.

41 Y. S. Oh, J. J. Yang, Y. Horibe, and S. W. Cheong, Phys. Rev. Lett. **110**, 127209 (2013), arXiv: 1303.4772.

42 C. Soulard, P. E. Petit, P. Deniard, M. Evain, S. Jobic, M. H. Whangbo, and A. C. Dhaussy, J. Solid State Chem. **178**, 2008 (2005).

43 Y. Zhang, C. Wang, L. Yu, G. Liu, A. Liang, J. Huang, S. Nie, X. Sun, Y. Zhang, B. Shen, J. Liu, H. Weng, L. Zhao, G. Chen, X. Jia, C. Hu, Y. Ding, W. Zhao, Q. Gao, C. Li, S. He, L. Zhao, F. Zhang, S. Zhang, F. Yang, Z. Wang, Q. Peng, X. Dai, Z. Fang, Z. Xu, C. Chen, and X. J. Zhou, Nat. Commun. **8**, 15512 (2017), arXiv: 1602.03576.

44 H. Chi, C. Zhang, G. Gu, D. E. Kharzeev, X. Dai, and Q. Li, New J. Phys. **19**, 015005 (2017), arXiv: 1701.04737.

45 J. Banhart, Phys. Rev. B **53**, 7128 (1996).

46 W. Zheng, R. Schönemann, N. Aryal, Q. Zhou, D. Rhodes, Y. C. Chiu, K. W. Chen, E. Kampert, T. Förster, T. J. Martin, G. T. McCandless, J. Y. Chan, E. Manousakis, and L. Balicas, Phys. Rev. B **97**, 235154 (2018), arXiv: 1805.00087.